6

Variability of Internal Solitary Waves in the Northwest South China Sea

Zhenhua Xu and Baoshu Yin
Institute of Oceanology, Chinese Academy of Sciences,
Key Laboratory of Ocean Circulation and Waves (KLOCAW),
Chinese Academy of Sciences,
China

1. Introduction

Internal waves are waves that travel within the interior of the water column. Its existence is owned to the stratified density structure between two or continuous layers of fluids (Apel et al., 1987). Internal solitary waves (ISWs) are nonlinear internal waves, which are frequently observed all over the world oceans, where strong tides and stratification occur over varying topography features (Apel et al., 1985; Colosi et al., 2001; Osborne & Burch, 1980). They typically occur in packets at tidal intervals, suggesting that they mainly originate from the tide-topography interactions over variable topography (Gerkema et al., 1995). Depending on the different environmental conditions, there are two main mechanisms for the generation of ISWs: lee-wave mechanism (Maxworthy, 1979) and nonlinear internal tide mechanism (Lee & Beardsley, 1974).

The lee-wave mechanism states that the lee-wave is formed by the ebb tide and released when the tide changes from ebb tide to flood tide, and evolves into a rank-ordered internal solitary wave (ISW) packet. By the nonlinear internal tide mechanism, internal tides spawn ISWs in three steps: initial generation of a front due to topographic blocking, nonlinear steepening of the front, and formation of a rank-order ISW packet under effects of nonlinearity and dispersion (Helfrich & Melville, 2006; Zhao & Alford, 2006).

Internal solitary waves are important for many practical reasons. As they are commonly observed wherever strong tides and stratification occur next to the irregular topography, thus they are often prominent features seen in optical and radar satellite imagery of coastal waters. They can propagate over several hundred kilometers and transport both mass and momentum. They can also induce considerable velocity shears that can impose unexpectedly large stresses on offshore oil-drilling rigs and lead to turbulence and mixing. In addition, the mixing often introduces bottom nutrients into the water column, thereby fertilizing the local region and modifying the biology system therein (Jackson, 2004).

ISWs in the South China Sea (SCS) have been observed at a variety of locations from Luzon Strait to the continental shelf (Cai et al., 2002; Lien et al., 2005; Liu et al., 2004; Ramp et al., 2004; Xu et al., 2010; Zhao et al., 2004). Until recently, considerable effort has been focused on the study of ISWs in the northeastern SCS (Farmer et al., 2009; Moore et al., 2007; Ramp et al., 2004). In contrast, Due to the shortage of high-quality data sets, studies of the ISWs in the northwestern SCS are quite limited and nonlinear internal waves in this region have been

observed mainly by satellite remote sensing (Liu et al., 1998; Jackson, 2004; Li et al, 2008). Thus few attempts have been done on the statistical analysis of the ISWs and detailed study of the features of ISWs in this area based on long-term observations is rarely reported. In order to investigate the typical characteristics of ISWs in Wenchang area of the northwestern SCS, the Wenchang Internal Wave Experiment (WCIWE) was conducted in 2005. A complete set of current and temperature data of mooring measurements were acquired and numerous ISWs were observed in Wenchang area during this experiment. Based on the newly-acquired observation data, a prelimary study of the ISWs has been undertaken in this area (Xu et al., 2010). This chapter intends to present a summary of the interesting observations of the ISWs in the northwestern region, investigate the statistical characteristics of the ISWs, make a theoretical analyse using the KdV models and examine the possible effects of the ISWs on the platforms and marine biological system in the SCS.

2. Theoretical description of internal solitary waves

The earliest recognition of internal solitary wave phenomena was reported by Scott Russell (1838, 1844) in the 19th century. Later Korteweg and devries (1895) derived some of the interesting mathematical properties of such wave and produced the now-famous analytical soliton solutions. Despite the fact that the oceanic observations show the presence of mode-one internal waves that are often highly nonlinear, weakly nonlinear KdV-type theories have played the primary role in elucidating the essential features of the observations, if not always the precise quantitative details. They have the advantage of permitting modeling of unsteady wave evolution under various conditions with reduced wave equations (Helfrich and Melville, 2006; Koop and Butler, 1981; Small and Hornby, 2005).

The Korteweg and devries (KdV) equation arises from an assumption that nonlinearity, scaled by $\alpha = a/H$, and nonhydrostatic dispersion, $\beta = (l/H)^2$, are comparable and small: $\beta = O(\alpha) << 1$. Here a is a measure of the wave amplitude, H is an intrinsic vertical scale, and l is a measure of the wavelength (Holloway et al , 1997; Liu et al., 1998).

$$\frac{\partial \eta}{\partial t} + c\frac{\partial \eta}{\partial x} + \alpha\eta\frac{\partial \eta}{\partial x} + \beta\frac{\partial^3 \eta}{\partial x^3} = 0 \tag{1}$$

For a two-layer system with a rigid lid and no mean flow, in the Boussinesq approximation,

$$\alpha = \frac{3}{2}\frac{H_1 - H_2}{H_1 H_2}C_0 \tag{2}$$

$$\beta = \frac{1}{6}H_1 H_2 C_0 \tag{3}$$

$$C_0 = \left[\frac{\Delta\rho g H_1 H_2}{\rho(H_1 + H_2)}\right]^{\frac{1}{2}} \tag{4}$$

Here g is the gravitational acceleration, $\Delta\rho = \rho_2 - \rho_1$ is the layer density difference, ρ_1 (ρ_2) is the density of the upper (lower) layer, and H_1 and H_2 are the mean upper and lower layer depths, respectively. This equation has the solution:

$$\eta = \eta_0 \mathrm{sech}^2\left(\frac{x - Ct}{\lambda}\right) \tag{5}$$

The nonlinear velocity C and the characteristic width λ of the soliton being related to the linear speed C_0 and the amplitude of the displacement η_0 by

$$\mathrm{C} = C_0 + \frac{\alpha\eta_0}{3}, \quad \lambda^2 = \frac{12\beta}{\alpha\eta_0}. \tag{6}$$

When the interface is close to the middle of the water layer, $H_1 \approx H_2$,the nonlinear coefficient α is small or even equal to zero. In this case, high-order nonlinear coefficient must be included in the KdV equation, which results into the extended Korteweg-de Vries (eKdV) equation.

$$\frac{\partial\eta}{\partial t} + (c + \alpha\eta + \alpha_1\eta^2)\frac{\partial\eta}{\partial x} + \beta\frac{\partial^3\eta}{\partial x^3} = 0 \tag{7}$$

Where for the case of two-layer fluid the second nonlinear coefficient is

$$\alpha_1 = \frac{3c}{h_1{}^2 h_2{}^2}\left[\frac{7}{8}\left(\frac{\rho_2 h_1{}^2 - \rho_1 h_2{}^2}{\rho_2 h_1 - \rho_1 h_2}\right) - \frac{\rho_2 h_1{}^3 - \rho_1 h_2{}^3}{\rho_2 h_1 + \rho_1 h_2}\right] \approx -\frac{3}{8}\frac{(h_1 + h_2)^2 + 4h_1 h_2}{(H_1 H_2)^2} C_0 \tag{8}$$

With α_1=0 this reduces to the well-known KdV equation. This equation has a solitary wave solution of the form

$$\eta(x,t) = \eta_0 \frac{\sec h^2[\kappa(x - C_m t)]}{1 - \mu\tanh^2[\kappa(x - C_m t)]} \tag{9}$$

Where t is time, and x is the spatial variable in the direction of wave propagation. η_0 is the maximum interface elevation at x = 0, and κ and μ are parameters.
The characteristic wave-width λ predicted by the EKdV model is related to the mass of the wave by computing

$$\lambda = \frac{1}{2\eta_0}\int_{-\infty}^{\infty}\eta(x)dx \tag{10}$$

As follows from Eq. 8, within the framework of the two-layer model, α_1 is always negative. However, in the general case the coefficient α may be either negative or positive. In the latter case, solitons of both positive and negative polarities may exist. In addition, nonstationary solitons, called breathers, are also possible. The evolution of initial pulse-type perturbations may be fairly complex. If the pycnocline is located just at the critical level so that the parameter is exactly zero, Eq.7 reduces to the well-known modified Korteweg–de Vries （mKdV） equation.

$$\frac{\partial\eta}{\partial t} + (c + \alpha_1\eta^2)\frac{\partial\eta}{\partial x} + \beta\frac{\partial^3\eta}{\partial x^3} = 0 \tag{11}$$

The mKdV equation also has soliton-type solutions, but only those propagating on a constant nonzero pedestal (Apel et al., 2006).

3. Internal solitary waves in the northeast SCS

Based on their different characteristics, Ramp et al. (2004) denoted the two types of ISW packets on the slope of the northeastern SCS as a-wave and b-wave, respectively. The a-wave arrives with remarkable regularity at the same time each day, 24 hours apart; the b-wave arrives one hour later each day. The ISWs in the a-wave packets have greater amplitude than those in the b-wave packets. For the a-wave, the largest ISW is always in the lead with smaller ISWs behind, sometimes rank-ordered and sometimes not. The b-wave generally consists of a single ISW growing out of the center of the packet (Klymak et al., 2006; Zhao & Alford, 2006).
ISWs in this area appear to originate near the Luzon Strait and propagate westward across the SCS basin until they encounter the shelf near China's coast (Zhao & Alford, 2006). Liu et al. (1998) have studied the elevation ISWs east of Hainan Island by SAR images on the basis of the assumption of a semidiurnal tidal origin. They inferred that the wave packets were transformed from the depression ISWs generated near the Luzon Strait.
Large amplitude ISWs in the northeastern South China Sea (SCS) have been frequently reported since the Asian Seas International Acoustics Experiment. Hence, there has been an increasing interest in investigating the highly nonlinear effects on the ISWs in different models (Ramp et al., 2004; Farmer et al., 2009). As pointed by Ramp et al. (2004), simulating large amplitude ISWs in the northeastern SCS is limited in the EKdV model, but KdV theory is more suitable for the simulation of the solitons in this area.

4. Internal solitary waves in the northwest SCS

4.1 Observational methods

Field observations were made from late Spring to early Autumn 2005 at Wenchang Station (112°E, 19°35'N) on the northwestern shelf of the SCS. The water depth at the station is 117 m.

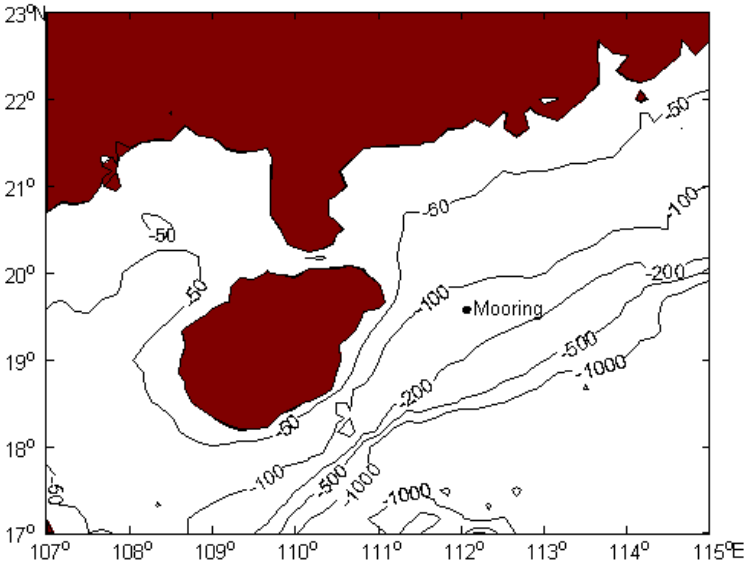

Fig. 1. Map of the study area with isobaths showing the seafloor topography Contours mark isobaths in meters. Symbol * indicates the mooring position.

The study area and mooring position are indicated in Fig.1. An array of temperature and salinity sensors, and an acoustic Doppler current profiler (ADCP) were deployed at Wenchang Station to examine the thermal and hydrodynamic structure on the Wenchang shelf. A 190 kHz down-looking ADCP was positioned at a depth of 8 m. The depth of the available current data measured by ADCP ranged from 10 to 114 m, with a vertical interval of 2 m. Current measurements were recorded with a precision of 1×10-4 m/s at a time interval of 10 min. The temperature sensor information with a precision of 0.01°C and a time interval of 1 min were collected at 23 layers. Most of the temperature sensors were placed between 4 and 40 m below the sea surface with a vertical separation of less than 4 m, whereas the bottom two sensors were located at depths of 50 and 75 m. Salinity measurements taken at a interval of 1 min were acquired at five layers by sensors placed at 8, 20, 30, 40, and 75 m (Xu et al., 2011).

4.2 Characteristics of the ISWs

4.2.1 General description of the ISW packets

In order to investigate the properties of the ISWs, the temperature data were converted to vertical displacements of isotherms using linear interpolation method. The semidiurnal tide dominated at the beginning of the observed record while the diurnal tide gradually became more pronounced on Sep 9-13, followed by semidiurnal tide again on Sep 14 and 15 (Figure 2a). In general, the ISWs occurred during the entire observation period, while the largest waves were observed once every diurnal tidal cycle from Sep 9 to 13 and the smaller waves were found to occur irregularly at roughly semidiurnal period. The dominate diurnal ISWs in our study area, with the possible local generation mechanism,are quite different from the principal solitons observed every semidiurnal tidal cycle in the northeastern SCS (Ramp et al., 2004).

Figure 2b shows three abrupt deepening of the upper stratified layer followed by developed packets of high-frequency ISWs. The regular arrival of internal wave packets riding on these depression bores of strong tides at roughly the diurnal tidal period strongly suggests that the main energy source of the waves is the diurnal tide. The internal tides on 10 and 11 September are obviously stronger than that of 9 September.

The seasonal thermocline, generally between 20 m and 50 m depth during this period, was deepened more than twenty meters by the strong internal tides and ISWs (Figure 2c). The strongest stratification of the water column appears around 05:00 on 10 September when the temperature gradient reaches as large as 0.55 ℃/m. The most noticeable difference is that the thermocline on 9 September is relatively weaker than that of 10 September through the whole observed water column. Therefore, the ISWs display distinct characteristics during these two days, which will be discussed in the next section.

4.2.2 Depression internal solitary waves

A closer inspection of the time series of temperature data for 9 September is shown to get a better view of the internal wave structure. Figure 3a shows an internal tide steepening trailed by a packet of ISWs. The first soliton emerged on the front face of the internal bore. The spike-like fluctuation of temperature first increased and then decreased. This indicates that the solitons are depression waves. The temperature fluctuates in phase vertically for the entire water column, which suggests that these solitons all behave as the first mode depression waves. The largest soliton appears around 12:15 on 9 September with the amplitude and period of order 25 m and 20 min, respectively (Figure 3b). There are several small solitons appearing before and after the main soliton.

Before the ISWs arrived, the average temperature in the upper mixed layer was about 28.5 ℃ and the mixed layer thickness was roughly 25 m in the water of 117 m depth (Figure 3c). Below the upper mixed layer, there was a strong thermocline with the temperature gradient of 0.35 ℃/m. When the main soliton arrived around 12:15 on 9 September, the temperature structure changed dramatically with the mixed layer deepened to 50 m depth. This result again confirms our previous description that the amplitude of the main soliton is approximately 25 m.

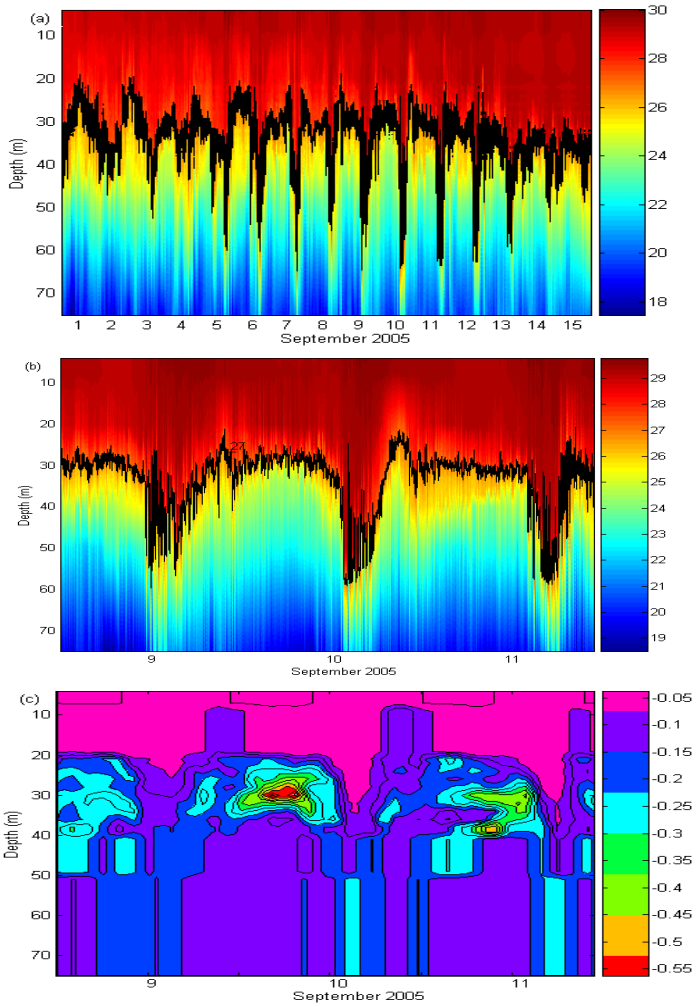

Fig. 2. (a) 15-day time series of isotherm depths from the temperature data from September 1 to September 15, 2005. The isotherm of 27 ℃ is noted, (b) 3-day time series of isotherm depths from the temperature data from September 9 to September 11, 2005. The isotherm of 27 ℃ is noted, (c) 3-day time series of temperature gradient depths from September 9 to September 11, 2005. After Xu et al. (2010).

The largest soliton arriving around 12:15 on 9 September was classic mode-1 wave, with opposing velocities in the upper and lower layers (Figure 3d). The point of the zero crossing of the velocity was close to 55 m, which was associated with the strong thermocline during the arrival of the main soliton indicated by figure 3c. The direction of the horizontal velocity changed with depth, roughly northwestward in the upper layer and southeastward in the lower layer. According to the KDV theory of the ISW, the direction of the depression ISW is the same as that of the currents in the upper layer water column. These results suggest that this soliton behaves as the first mode depression wave, propagating nearly northwestward.

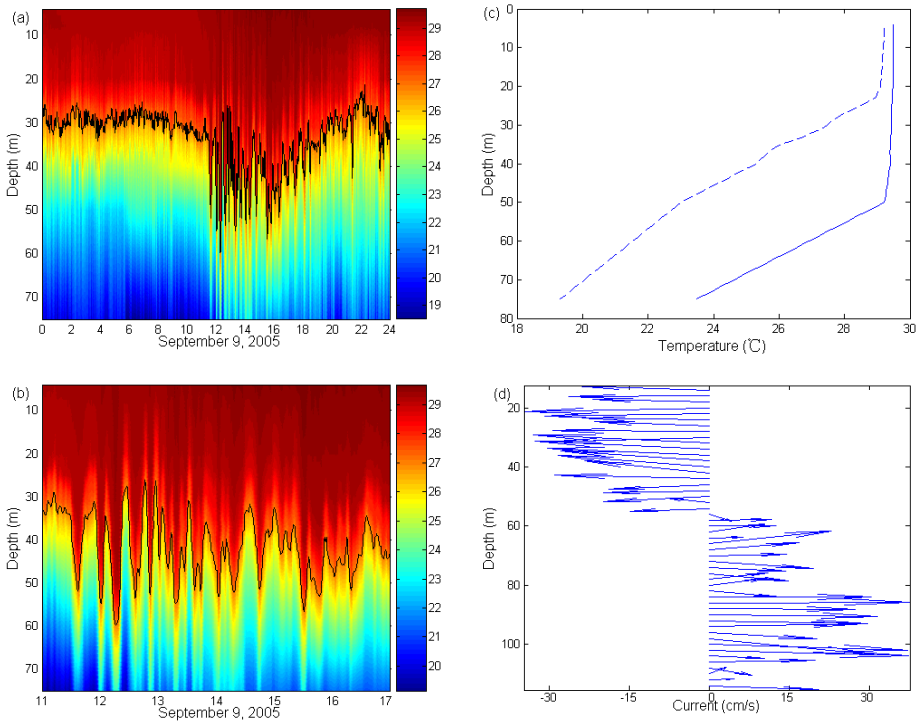

Fig. 3. 24-h (a) and 6-h (b) time series of isotherm depths from the temperature data on September 9, 2005. The isotherm of 27 ℃ represents the thermocline, (c) Temperature profiles measured before and during the passing of largest soliton which appears around 12:15 on 9 September. The dashed line indicates the profiles obtained by averaging the temperature data from 10:20 to 10:40 on 9 September, while the solid line indicates the profiles during the passing of this soliton, (d) ISW current speed around 12:15 on 9 September obtained by high-pass filtering the raw current data with a 3-h cutoff period. The arrows denote the vectors of current speed. Upward direction of the arrow is due the North. After Xu et al., (2010).

4.2.3 Elevation internal solitary waves

The ISWs on 10 September have similar characteristics to the September 9 solitons, but there are also some remarkable and interesting differences. Figure 4a shows an abrupt deepening of the upper stratified layer followed by several rank-ordered solitons. The temperature also fluctuated in phase vertically for the whole observed water column. The waves are rank-ordered in amplitude with the largest soliton in the lead. The remarkable feature to notice is the occurrence of elevation waves riding on top of a large depression bore. The spike-like fluctuation of temperature shows they first decrease and then increase, which indicates that the solitons are elevation waves. The largest wave arriving around 14:50 on 10 September with amplitude and period of order 35 m and 15 min was consistent with the elevation wave of first mode (Figure 4b).

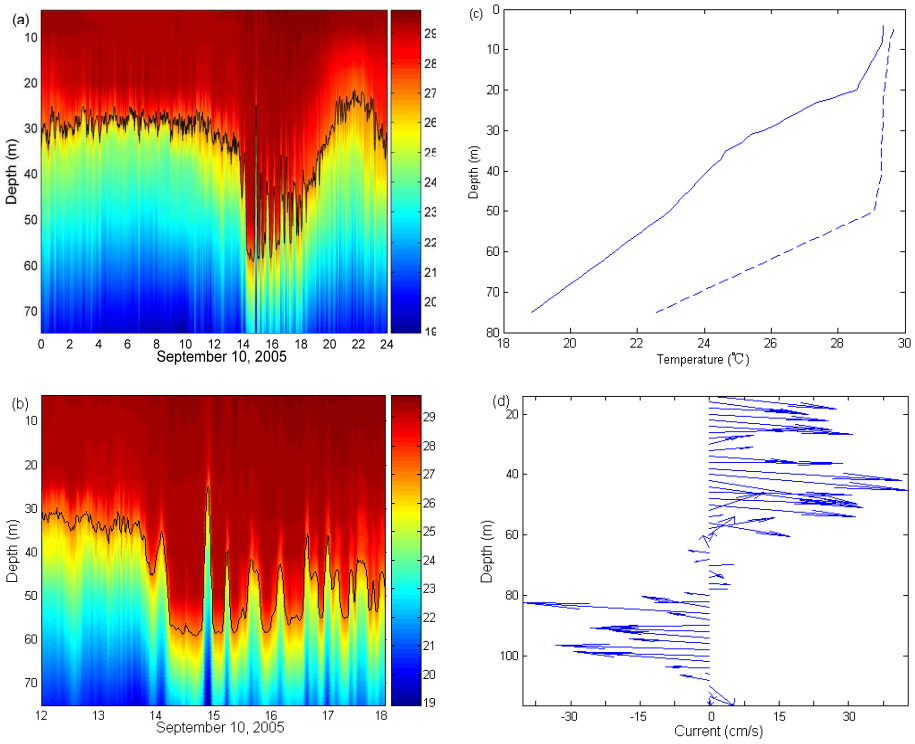

Fig. 4. 24-h (a) and 6-h (b) time series of isotherm depths from the temperature data on September 10, 2005. The isotherm of 27 ℃ represents the thermocline, (c) Temperature profiles measured before and during the largest soliton which appears around 14:50 on 10 September. The dashed line indicates the profiles obtained by averaging the temperature data from 14:20 to 14:40 on 10 September; while the solid line indicates the profiles during the passing of this soliton, (d) ISW current around 14:50 on 10 September obtained by high-pass filtering the raw current data with a 3-h cutoff period. After Xu et al., (2010).

Before the ISWs arrived, the average temperature in the upper mixed layer was about 29 ℃ and the mixed layer thickness was about 60 m in the water of 117 m depth due to the passing of a large depression bore. Below the upper mixed layer, there was a strong thermocline with the temperature gradient of 0.25 ℃/m. When the main soliton arrived around 14:50 on 10 September, the mixed layer was raised to 20 m (Figure 4c). This again confirms our previous observation that the amplitude of the main soliton is more than 35 m. The largest soliton arriving around 14:50 on 10 September was also classic mode-1 wave, with opposing velocities in the upper and lower layers (Figure 4d). The vertical location of the zero crossing of the velocity was between 60 m and 80 m. This soliton has opposite polarity to the ISWs appearing on 9 September. The current directions in the upper and lower layers were eastward with slightly southward and westward with slightly northward respectively. According to the KDV theory of the ISW, the elevation ISWs propagate in the same direction as that of the currents in the lower layer water. These results indicate that the September 10 soliton also propagate mainly westward, but deflect slightly to the north. However, on the contrary to the solitons on 9 September, the solitons on 10 September behave as mode-1 elevation waves due to the passing of a large depression of tidal bore.

This type of elevation ISWs observed on 10 September during WCIWE is not unique. However, it's exciting and interesting that both elevation and depression ISWs were observed at the same mooring location in different days. There were several similar wave packets propagating roughly northwestward from 9 September to 13 September, 2005. These wave packets were observed around the time of the spring tides in the study area. The seasonal thermocline generally locates at a constant depth during a short period, and the upper mixed layer of 30 m during the autumn is usually thinner than the bottom layer on the shelf of the northwestern SCS. However, the study area is dominated by the diurnal internal tides with the amplitude of 30 m much larger than that caused by the semidiurnal semidiurnal tides. There exists the possibility of a location at which the thermocline of these tidal bores with depression of 30 m is closer to the bottom than to the surface. Prior to the arrival of the ISWs during 10 September, the thermocline lowered progressively owning to the strong diurnal internal tide. So, the upper layer thickness of 60 m almost exceeded the bottom layer thickness of 57 m in the wake of this sudden depression, and the elevation waves were expected to be evolved from the internal tides due to the changing sign of nonlinear effects at this critical depth according to the theory of ISWs. On the contrary, the diurnal tide on 9 September is a little weaker than that on 10 September, the thermocline was slightly above mid-depth even during the trough of the internal tides and so the usual depression waves formed. The largest elevation soliton on 10 September with the amplitude of 35 m was very strong in related to the total depth of 117 m. The high energy of this type of elevation ISW must be important for sediment resuspension (Bogucki et al., 1997; Klymak et al., 2003) and in the energy budget. Hsu et al. (2000) have demonstrated using KdV-type numerical model that both depression and elevation waves can be generated in the upwelling area dependent on the stratification and the initial tidal mixing condition near the generation area. In the next section, we will also use the KdV equations to investigate the nonlinear effects, and then demonstrate the significant role of the ISWs in affecting the platform and biological system in the ocean interior.

4.3 Theoretical analysis of the highly ISWs

4.3.1 General description of the highly ISW packets

During the WCIWE experiment, as described in the former section, extremely strong ISWs were observed frequently. The maximum amplitude of the ISWs during the observational period reached as much as 45 m, which are the largest internal waves that have been observed in this area, which suggests that the highly nonlinear ISWs in the northwestern SCS are an indispensable part of the energy budget of the internal waves in the northern SCS. A detail study on the 3-h time series of temperature for May 5 (Figure 5) provides a good view of the internal wave structure. The prominent feature to note for the ISWs on May 5 is that the large soliton extending down from the leading edge of the low frequency wave displacement by up to 45 m. In addition, several small solitons appeared before and after the main soliton. Furthermore, it is apparently to see that larger waves have longer wave periods, to which we will discuss in detail in the next section.

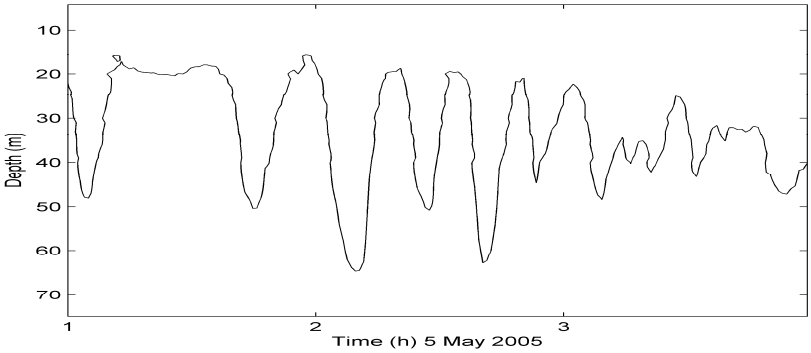

Fig. 5. 3-hour time series of 25°C isotherm depths from the temperature data for 5 May 2005.

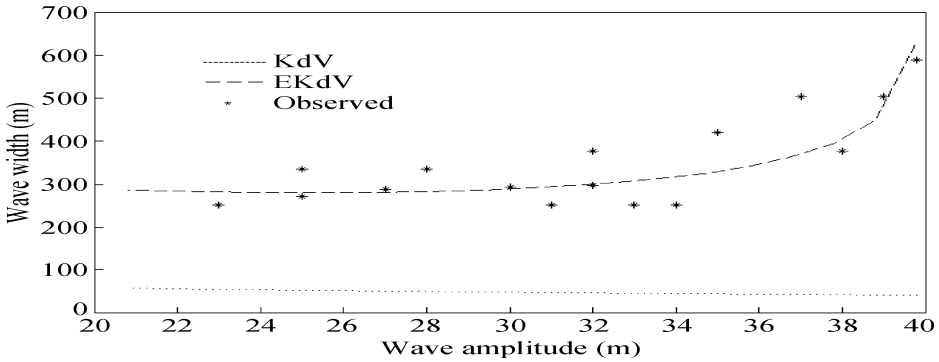

Fig. 6. Wave widths versus wave amplitude for observed ISWs. The prediction from the EKdV and KdV theory are plotted for reference. After Xu et al., (2010).

4.3.2 Theoretical analysis

Michiallet et al. (1998) showed in their laboratory experiment that large amplitude waves can be better approximated by the second-order EKdV, (formed by including the cubic non-linear term) than by the KdV theory. Based on the observation in the northwestern SCS, we investigated high-order nonlinear effects on the depression solitary waves by comparing the solutions of EKdV model in first-order KdV theory.

The relationship between the wave widths and amplitude is an important characteristic for an ISW and represents the most fundamental difference between various theories and the observation (Koop et al., 1980). Thus, the classical KdV and EKdV solutions were compared to the observed width of ISWs with moderate to large amplitudes. The widths of these waves are plotted against wave amplitude (Figure 6). The environmental parameters used to derive the theoretical values include upper layer thickness of 30 m, lower layer thickness of 90 m, and density contrast of 3 kg m^{-3}. The wave widths were computed from the time durations measured between the points where the amplitude decayed to 0.42 times of the maximum amplitude, and converted wave widths were assumed at a constant linear phase speed of 0.7 m s-1 estimated from the KdV and EKdV theory (Colosi et al., 2001). As expected, it was found that the EKdV solutions produced a satisfactory fit to the scatter data. On the other hand, using classical KdV theory produced much narrower solitons than those by observation and by the EKdV computation. For example, waves in 117 m water depth between 20 and 40 m in amplitude and between 250 and 500 m in width are clustered around the analytical curve of the EKdV equation, while for KdV waves of 20 to 40 m in amplitude, the wave width is less than 50 m, suggesting that the classical KdV equation is incapable of simulating highly nonlinear solitons. In particular, wave width is expected to decrease linearly as wave amplitude grows based on the KdV equation. The EKdV equation, on the contrary, suggests that wave width increases with wave amplitude, which conforms well to the features of large amplitude ISWs observed during our experiment. These finding were similar to those of Michiallet et al. (1998) and Chen et al. (2007, 2008, 2009); they compared theoretical solutions with experimental data.

To provide some estimate of the variance between two profiles, two representative individual waveform at different amplitudes are compared and presented. By comparing observed wave profiles with those predicted by internal wave theory (Fig.7), the EKdV equation is shown to satisfactorily represent the ISW at moderate to large amplitudes. However, KdV theory predicted a much shallower width than what was observed. A remarkable feature to be investigated is that the width of the observed wave grows with the amplitude, which fits well with the wave width predicted by EKdV. In contrast, the predicted width by KdV decreases with increasing amplitude and does not capture the broadening of observed waves, i.e., the KdV solution deviates more from the observation as the wave grows. This phenomenon may be due to the fact that in this shallow water situation, the wave pushes the thermocline down to a region where the nonlinear coefficients in KdV approach zero, under which the KdV theory does not predict the presence of ISWs. As mentioned previously, the EKdV theory with an extra cubic nonlinear term is particularly appropriate for this situation. Therefore, we suggest that the discrepancy between the observations and the KdV theory wave shape is likely due to high-order cubic nonlinear effects. The cubic nonlinear terms become more important than the quadratic nonlinear term and should not be neglected in simulation of large amplitude ISWs on continental shelves.

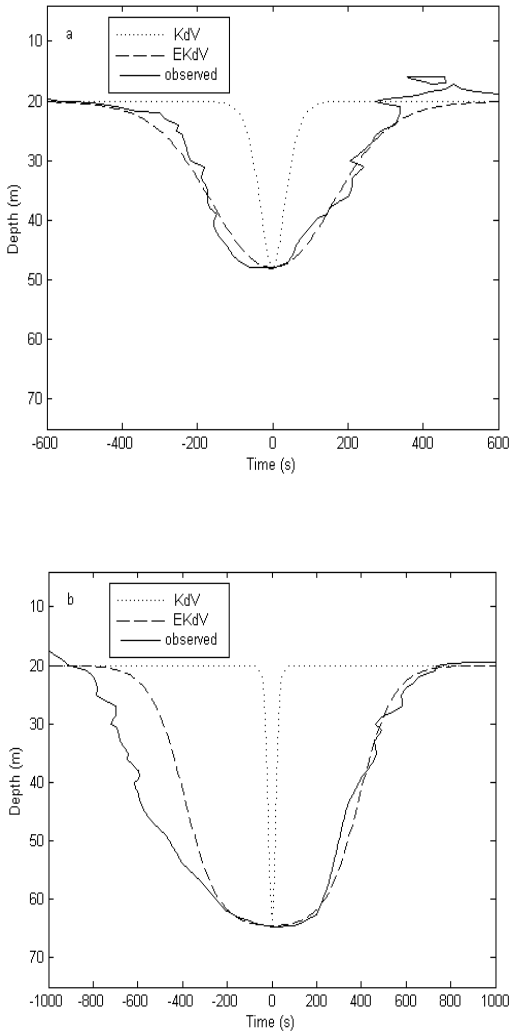

Fig. 7. Observed wave shapes in different amplitudes from May 1 at 28 m (a) and 5 May at 45 m (b)The prediction from the EKdV and KdV theory are plotted for reference. After Xu et al., (2010).

However, as pointed by Ramp et al. (2004), simulating large amplitude ISWs in the northeastern SCS is limited in the EKdV model. This is because large amplitude waves in deep water (>500 m) do not push the thermocline deep enough in a water column, and therefore the effect of the cubic nonlinear term on the soliton is less important than that of the quadratic nonlinear term. Hence, the EKdV model is less appropriate in this situation (Fan et al., 2008). However, as we described above, for highly nonlinear ISWs in shallow

water, such as on the shelf of the northwestern SCS where the ratio of the cubic nonlinear term to the quadratic nonlinear term becomes much greater than those in deep water, the EKdV model is more suitable.

4.4 Effects on marine biological variations

Internal waves might play an important role in affecting the nutrient regeneration in a tropical reef ecosystem. Unfortunately, we are unable to acquire the chlorophyll and dissolved oxygen data during our experiment. However, in the northeastern SCS, previous studies have highlighted the significant effects of the internal waves on the reef ecosystem, based on the field measurements at Dongsha Atoll in the northern SCS (Wang et al., 2007). They found that mixing and advection by internal waves could generate upward flues of nutrients and suggested that the episodic upwelling of deep water due to internal waves might account for the high coral cover on the shallow reef slopes of Dongsha Atoll, in contrast to the extreme high mortality of corals inside the lagoon that occurred during the 1997-98 EI Eino warming event. Further studies based on more field measurement data are needed to quantify the temporal and spatial variations of nutrients and microbial abundance to demonstrate the ecological effects of internal waves in the coral reef ecosystem.

4.5 Wave-induced force on a pile

Based on first-order KdV theory, Cai et al. (2003) introduced Morison's empirical formula to estimate the forces and torques exerted by ISWs on cylindrical piles near Dongsha Islands in the northeastern SCS (Cai et al., 2008; Morison et al., 1950). However, as we have described above, classical KdV equation was completely inapplicable for the simulation of highly nonlinear solitons in the northwestern SCS, whereas EKdV equation could satisfactorily represent the ISW in moderate to large amplitude in this area. As a result, in this section, we use EKdV theory to estimate the induced current by the ISWs based on the Morison formula (See Cai et al., 2003 for details), and then calculate the wave force on a cylindrical pile in the northwestern SCS.

The results show that the horizontal current induced by the soliton reverse the direction in the upper and lower layer, and the maximum current speed in the lower layer is smaller than that in the upper layer. Similarly, the wave forces acting on the pile also reverse their directions due to the variation of the horizontal velocity and the maximum wave forces are 300 kN and 100 kN for the upper layer and the lower layer, respectively.

5. Conclusion

Based on the observation data of ADCP and thermistor chain, an unprecedented detailed study of the ISWs on the continental shelf of the northwestern South China Sea has been presented. Both elevation and depression ISWs are observed and behave as the first mode nonlinear wave in the mooring area. The ISWs occur at the interval of diurnal frequencies, which are distinctly different from the ISW in the northeastern area, where the solitons mainly appear with the semi-diurnal frequency, suggesting that the ISWs in the northwestern SCS might be generated by the local tide-topography interactions. In addition, a highly nonlinear wave was observed to displace the thermocline down to 45 m, making it the largest wave that was ever observed in this area. Furthermore, the comparison between the results of theoretical predictions and observations shows that the high nonlinearity of

the depression waves is represented by second-order EKdV theory better than first-order KdV theory. Maximum internal wave forces on a cylindrical Pile on the northwestern shelf of SCS are estimated to be 300 kN and 100 kN for the upper layer and the lower layer, respectively. Thus, the ISWs in our study area can cause serious threat to ocean engineering structures. In addition, mixing and advection by internal waves were found to generate upward flues of nutrients and affect the nutrient regeneration in a tropical reef ecosystem. Further measurements and numerical simulations are needed to study the generation mechanism of the solitons and to demonstrate the ecological effects of internal waves in the coral reef ecosystem.

6. Acknowledgment

This work is supported by National Natural Science Foundation of China (No. 41106017 and No. 41030855), Key program of Knowledge Innovation Project of Chinese Academy of Sciences (No.KZCX1-YW-12), Natural Science Foundation of Jiangsu Province of China (BK2011396), and the National 863 program (No. 2008AA09A401).

7. References

Apel, J.R. (1987). *Principles of ocean physics*, Academic Press, Ltd., London, 634pp.

Apel, J.R.; Holbrook, J. R.; Liu, A. K. & Tsai J. J. (1985). The Sulu Sea internal soliton experiment. *J. Phys. Oceanogr.*, 15: 1625– 1651.

Apel, J.R.; Ostrovsky, L.A.; Stepanyants, Y.; & Lynch, J.F. (2007). Internal solitons in the ocean and their effect on underwater sound. *Journal of the Acoustical Society of America*, 121(2): 695-722.

Baines, P.G. (1982). On internal tide generation models. *Deep Sea Res.*, 29: 307–338.

Bogucki, D.J.; Redekopp, L. & Dickey, T. (1997). Sediment resuspension and mixing by resonantly generated internal solitary waves. *J. Phys. Ocean.*, 27: 1181-1196.

Cai, S.; Gan, Z. & Long, X. (2002). Some characteristics and evolution of the internal soliton in the northern South China Sea. Chin Sci Bull, 47(1): 21-26.

Cai, S.Q.; Long, X.M. & Gan, Z.J. (2003). A method to estimate the forces exerted by internal solitons on cylindrical Piles. Ocean Engineering, 30: 673-689.

Cai, S.Q.; Long, X.M. & Wang, S.A. (2008). Forces and torques exerted by internal solitons in shear flows on cylindrical piles. Applied Ocean Research, 30: 72–77.

Chen, C.Y. (2009) Amplitude decay and energy dissipation due to the interaction of internal solitary waves with a triangular obstacle in a two-layer fluid system: the blockage parameter. Journal of Marine Science and Technology, 14(4): 499-512.

Chen, C.Y.; Hsu, J.R.C.; Cheng, M.H. & Chen, C.W. (2008). Experiments on mixing and dissipation in internal solitary waves over two triangular obstacles. Environmental Fluid Mechanics, 8(3): 199-214.

Chen, C.Y.; Hsu, J.RC. & Cheng, M.H. 2007. An investigation on internal solitary waves in a two-layer fluid: Propagation and reflection from steep slopes. *Ocean Engineering*, 34(1): 171-184.

Colosi, J.A.; Beardsley, R.C.; Lynch, J.F.; Gawarkiewicz, G.; Chiu, C.S. & Scotti, A. (2001). Observations of nonlinear internal waves on the outer New England continental shelf during the summer Shelf break Primer study. *J. Geophys. Res.*, 106: 9587– 9601.

Duda,T.F.; Lynch, J.F.; Irish, J.D.; Beardsley, R.C.; Ramp, S.R.; Chiu, C.S.; Tang, T.Y. & Yang, Y.J. (2004). Internal tide and nonlinear internal wave behavior at the continental slope in the northern South China Sea. *IEEE J. Oceanic Eng*., 29: 1105–1130.

Fan, Z.S.; Zhang, Y.L. & Song, M. (2008). A study of SAR remote sensing of internal solitary waves in the north of the South China Sea: I. Simulation of internal tide transformation. Acta Oceanologica Sinica. 27(4): 39-56.

Fan, Z.S.; Zhang, Y.L. & Song, M. (2008). A study of SAR remote sensing of internal solitary waves in the north of the South China Sea: II. Simulation of SAR signatures of internal solitary waves. Acta Oceanologica Sinica. 27(5): 36-48.

Farmer, D.; Li, Q. & Park, J.H. (2009). Internal Wave Observations in the South China Sea: The Role of Rotation and Non-Linearity. *Atmosphere-Ocean*, 47(4): 267-280.

Gerkema, T., & Zimmerman, J. T. F. (1995). Generation of nonlinear internal tide and solitary waves. *J. Phys. Oceanogr*., 25: 1081– 1094.

Grimshaw, R.; Pelinovsky, E. & Talipova, T. 2002. Higher-order Korteweg-de Vries models for internal solitary waves in a stratified shear flow with a free surface. *Nonlin. Processes Geophys*., 9: 221-235.

Helfrich, K.R. & Melville, W.K. (2006). Long nonlinear internal waves. *Annu. Rev. Fluid Mech.*, 38, 395–425.

Henyey, F.S. & Hoering, A. (1997). Energetics of borelike internal waves. *J. Geophys. Res*., 102: 3323– 3330.

Holloway, P.E.; Pelinovsky, E.; Talipova, T. & Barnes, B. (1997). A nonlinear model of internal tide transformation on the Australian north west shelf. J. Phys. Oceanogr., 1997,27:871-896.

Hsu, M.K.; Liu, A. K. & Liu, C. (2000). A study of internal waves in the China Seas and Yellow Sea using SAR. *Continental Shelf Res.*, 20: 389-410.

Jackson, C.R. (2004). An Atlas of Internal Solitary-Like Waves and Their Properties, 2nd ed., 560 pp., Global Ocean Assoc., Alexandria, Va. (Available at http://www.internalwaveatlas.com).

Klymak, J.M. & Moum, J. N. (2003). Internal solitary waves of elevation advancing on a shoaling shelf,. *Geophys. Res. Lett*., 30(20), 2045, doi:10.1029 /2003GL017706.

Klymak, J.M.; Pinkel, R.; Liu, C.T.; Liu, A.K. & David L. (2006). Prototypical solitons in the South China Sea. Geophys. Res. Letters, 33, L11607, doi:10.1029/ 2006GL025932.

Koop, C.G. & Butler, G.. (1981). An investigation of internal solitary waves in a two-fluid system. J. Fluid Mech., 112: 225-251.

Lee, C.Y. & Beardsley, R.C. (1974). The generation of long nonlinear internal waves in a weakly stratified shear flow. *J. Geophys. Res*., 79: 453– 462.

Li, X.; Zhao, Z. & Pichel, W.G. (2008). Internal solitary waves in the northwestern South China Sea inferred from satellite images. *Geophy. Res. Let*., 35, L13605, doi:10.1029/2008GL034272.

Lien, R.C.; Tang, T.Y.; Chang, M.H. & D'Asaro, E.A. (2005). Energy of nonlinear internal waves in the South China Sea, *Geophys. Res. Lett.,* 32, L05615, doi: 10.1029/2004GL022012.

Liu, A.K., & Hsu, M.K. (2004). Internal wave study in the South China Sea using synthetic aperture radar (SAR). *Int. J. Remote Sens*., 25: 1261– 1264.

Liu, A.K., Chang, Y.S.; Hsu, M.K. & Liang, N.K. (1998). Evolution of nonlinear internal waves in the East and South China Seas. *J Geophys Res*., 103(C4): 7995-8008.

Maxworthy, T. (1979). A note on the internal solitary waves produced by tidal flow over a three-dimensional ridge. *J. Geophys. Res*., 84: 338– 346.

Michallet, H.; Barthelemy, E. (1998). Experimental study of interfacial solitary waves. *Journal of Fluid Mechanics*, 366: 159-177.

Moore, S.E. & Lien, R.C. (2007). Pilot whales follow internal solitary waves in the South China Sea. *Marine Mammal Science*, 23(1): 193-196.

Morison, J.R.; O'Brien, M.P.; Johnson, J.W. & Schaaf, S.A. (1950). Forces exerted by surface waves on piles. AIME Petroleum Transactions. 189: 149-154.

Osborne, A. R., & Burch, T. L. (1980). Internal solitons in the Andaman Sea. *Science*, 208: 451–460.

Ramp, S.R.; Tang, T.Y.; Duda, T.F.; Lynch, J.F.; Liu, A.K.; Chiu, C.S.; Bahr, F.L.; Kim, H.R. & Yang, Y.J. (2004). Internal solitons in the northeastern South China Sea, Part I: Sources and deep water propagation, *IEEE J. Oceanic Eng*., 29: 1157– 1181.

Russell, J. S. (1838). Report of the Committee on Waves. Rep. Meet. British Assoc. Adv. Sci 7th, Liverpool. John Murray, London, 417-496.

Russell, J. S. (1844). Report on Waves. 14th Meeting Brit. Assoc. Adv. Sci., 311-390.

Small, R.J. & Hornby, R.P. (2005). A comparison of weakly and fully non-linear models of the shoaling of a solitary internal wave. Ocean Modelling, 8: 395–416.

Xu, Z.H.; Yin, B.S. & Hou, Y.J. (2010). Highly nonlinear internal solitary waves over continental shelf of northwestern South China Sea. *Chin.J.Oceanol.Limonol*, 28(5): 1049-1054.

Xu, Z.H.; Yin, B.S. & Hou, Y.J. (2011). Multimodal structure of the internal tides on the continental shelf of the northwestern South China Sea. Estuarine, Coastal and Shelf Science, doi:10.1016/j.ecss.2011.08.026.

Xu, Z.H.; Yin, B.S.; Hou, Y.J.; Fan, Z.S. & Liu, A.K. (2010). A study of internal solitary waves observed on the continental shelf in the northwestern South China Sea. *Acta Oceanologica Sinica*, 29:18-25.

Zhao, Z. & Alford, M. H. (2006). Source and propagation of internal solitary waves in the northeastern South China Sea. *J. Geophys. Res.,* 111, C11012, doi:10.1029/2006JC003644.

Zhao, Z.; Klemas, V.; Zheng, Q. & Yan, X. (2004). Remote sensing evidence for baroclinic tide origin of internal solitary waves in the northeastern South China Sea. Geophys. Res. Lett., 31. L06302, doi:10.1029/2003GL019077.

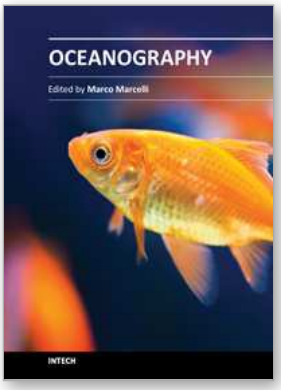

Oceanography

Edited by Prof. Marco Marcelli

ISBN 978-953-51-0301-1
Hard cover, 348 pages
Publisher InTech
Published online 23, March, 2012
Published in print edition March, 2012

How inappropriate to call this planet Earth when it is quite clearly Ocean (Arthur C. Clarke). Life has been originated in the oceans, human health and activities depend from the oceans and the world life is modulated by marine and oceanic processes. From the micro-scale, like coastal processes, to macro-scale, the oceans, the seas and the marine life, play the main role to maintain the earth equilibrium, both from a physical and a chemical point of view. Since ancient times, the world's oceans discovery has brought to humanity development and wealth of knowledge, the metaphors of Ulysses and Jason, represent the cultural growth gained through the explorations and discoveries. The modern oceanographic research represents one of the last frontier of the knowledge of our planet, it depends on the oceans exploration and so it is strictly connected to the development of new technologies. Furthermore, other scientific and social disciplines can provide many fundamental inputs to complete the description of the entire ocean ecosystem. Such multidisciplinary approach will lead us to understand the better way to preserve our "Blue Planet": the Earth.

How to reference

In order to correctly reference this scholarly work, feel free to copy and paste the following:

Zhenhua Xu and Baoshu Yin (2012). Variability of Internal Solitary Waves in the Northwest South China Sea, Oceanography, Prof. Marco Marcelli (Ed.), ISBN: 978-953-51-0301-1, InTech, Available from: http://www.intechopen.com/books/oceanography/variability-of-internal-solitary-waves-in-the-northwest-south-china-sea

INTECH
open science | open minds

InTech Europe
University Campus STeP Ri
Slavka Krautzeka 83/A
51000 Rijeka, Croatia
Phone: +385 (51) 770 447
Fax: +385 (51) 686 166
www.intechopen.com

InTech China
Unit 405, Office Block, Hotel Equatorial Shanghai
No.65, Yan An Road (West), Shanghai, 200040, China
中国上海市延安西路65号上海国际贵都大饭店办公楼405单元
Phone: +86-21-62489820
Fax: +86-21-62489821